Interaction of Cytochrome c with Cytochrome c Oxidase: An NMR Study on Two Soluble Fragments Derived from Paracoccus denitrificans †

ARTICLE *in* BIOCHEMISTRY · JUNE 2003

Impact Factor: 3.02 · DOI: 10.1021/bi027198f · Source: PubMed

7 AUTHORS, INCLUDING:

Oliver Maneg
Biotest Pharma GmbH
9 PUBLICATIONS **225** CITATIONS
SEE PROFILE

Primoz Pristovsek
National Institute of Chemistry
39 PUBLICATIONS **950** CITATIONS
SEE PROFILE

Interaction of Cytochrome *c* with Cytochrome *c* Oxidase: An NMR Study on Two Soluble Fragments Derived from *Paracoccus denitrificans*†

Hans Wienk,‡,⊥,|| Oliver Maneg,§,|| Christian Lücke,‡,# Primož Pristovšek,¶ Frank Löhr,‡ Bernd Ludwig,§ and Heinz Rüterjans*,‡

Institute of Biophysical Chemistry, J.W. Goethe-University, and Molecular Genetics, Institute of Biochemistry, J.W. Goethe-University, Marie-Curie-Strasse 9, D-60439 Frankfurt am Main, Germany, and National Institute of Chemistry, Hajdrihova 19, SI-1000 Ljubljana, Slovenia

Received November 19, 2002; Revised Manuscript Received March 17, 2003

ABSTRACT: The functional interactions between the various components of the respiratory chain are relatively short-lived, thus allowing high turnover numbers but at the same time complicating the structural analysis of the complexes. Chemical shift mapping by NMR spectroscopy is a useful tool to investigate such transient contacts, since it can monitor changes in the electron-shielding properties of a protein as the result of temporary contacts with a reaction partner. In this study, we investigated the molecular interaction between two components of the electron-transfer chain from *Paracoccus denitrificans*: the engineered, water-soluble fragment of cytochrome c_{552} and the Cu_A domain from the cytochrome *c* oxidase. Comparison of [^{15}N,^{1}H]-TROSY spectra of the [^{15}N]-labeled cytochrome c_{552} fragment in the absence and in the presence of the Cu_A fragment showed chemical shift changes for the backbone amide groups of several, mostly uncharged residues located around the exposed heme edge in cytochrome c_{552}. The detected contact areas on the cytochrome c_{552} surface were comparable under both fully reduced and fully oxidized conditions, suggesting that the respective chemical shift changes represent biologically relevant protein−protein interactions.

In the soil bacterium *Paracoccus denitrificans*, the electron transfer from complex III (cytochrome bc_1) to complex IV (heme aa_3-type cytochrome *c* oxidase) is mediated by the 18-kDa membrane-bound cytochrome c_{552} (*1*, *2*). In the second half of this shuttle pathway, the reduced cytochrome c_{552} interacts with the hydrophilic domain of subunit II of the oxidase. Positively charged lysine residues on the cytochrome c_{552} surface, clustered around its exposed heme edge, and patches of opposite charge above the binuclear Cu_A center in subunit II provide the basis for long-range electrostatic attractions that define the encounter complex (*3*). This is thought to be followed by a phase of molecular rearrangement that involves hydrophobic residues on the surface of both molecules, enabling the extra electron in the reduced heme of cytochrome c_{552} to be transferred to the Cu_A center, the first acceptor in the oxidase. This heme-to-copper electron transfer is mediated by tryptophan 121 at the contact surface of the oxidase subunit II (*4*).

The study of transient electron-transfer complexes in atomic detail is not straightforward. In vivo, protein−protein interactions during electron transfer are optimized to support high turnover numbers, implying that only transient complexes between the redox partners are formed. Moreover, due to fast redox equilibration in bimolecular complexes, the redox state of the individual components (electron donor and acceptor) is likely to be inhomogeneous under physiological conditions. For practical reasons, however, in vitro studies usually employ nonfunctional protein derivatives or use an excess of redox reagent to produce a homogeneous redox state.

Only a limited number of experimental techniques yield structural information on an atomic level. High-resolution NMR[1] spectroscopy has been established as a powerful method to obtain detailed three-dimensional structures of biomolecules. In addition, it is particularly useful for the topological analysis of transient complexes (e.g., refs *5* and *6*) and for the study of different redox states, since the chemical shifts observed in NMR spectra provide information on the electronic shielding of the observed nuclei.

† This work was supported by the European Union (grant no. QLG2-CT-1999−01003) and by the Deutsche Forschungsgemeinschaft (SFB 472). H.W. received a fellowship from the Alexander-von-Humboldt Foundation. P.P. received financial support from the Ministry of Education, Science and Sport of Slovenia.

* To whom correspondence should be addressed. E-mail: hruet@bpc.uni-frankfurt.de.

‡ Institute of Biophysical Chemistry, J.W. Goethe-University.

§ Molecular Genetics, Institute of Biochemistry, J.W. Goethe-University.

¶ National Institute of Chemistry, Slovenia.

⊥ Present address: Bijvoet Center for Biomolecular Research, Utrecht University, Padualaan 8, 3584 CH Utrecht, The Netherlands.

Present address: Max Planck Research Unit for Enzymology of Protein Folding, Weinbergweg 22, D-06120 Halle, Germany.

|| These authors contributed equally to the experiments reported in this study.

[1] Abbreviations: Cu_A, water-soluble Cu_A fragment of subunit II from *P. denitrificans* cytochrome *c* oxidase; *cyt* c_{552}, water-soluble domain of *P. denitrificans* cytochrome c_{552}; NMR, nuclear magnetic resonance; TROSY, transverse relaxation optimized spectroscopy.

10.1021/bi027198f CCC: $25.00
Published on Web 04/29/2003

Several chemical shift mapping analyses of electron-transfer protein complexes similar to *P. denitrificans* cytochrome c_{552}−cytochrome *c* oxidase have already been reported. For instance, Ubbink and Bendall (*7*) applied homonuclear NMR techniques to study the surface interactions between horse heart cytochrome *c* and pea plastocyanin, where the copper ion was replaced by cadmium in order to render the latter incapable of accepting electrons. Upon titration with one protein, the chemical shift changes of the backbone as well as side-chain amide protons of the other were monitored. Similarities in the results of the backbone and the side-chain resonance shifts were interpreted as the result of direct protein−protein contacts. For cytochrome *c* these were located around its exposed heme edge. In both proteins, certain residues showed backbone amide resonance shifts without concomitant changes in the side chains, indicating that complex formation can also affect nonsurface atoms of each reaction partner via transmittance of interaction effects to regions beneath the protein surface. In cytochrome *c* these residues were clustered within the positively charged region K86−R91, and in plastocyanin they were located around the cadmium ion (*7*).

Using a similar approach but a physiologically more relevant donor−acceptor combination, Worrall and co-workers (*8*) explained proton and nitrogen chemical shift changes of backbone amides as the result of the interaction between [^{15}N]-labeled yeast iso-1-cytochrome *c* and unlabeled yeast cytochrome *c* peroxidase. In both the fully reduced and the fully oxidized states, the most pronounced chemical shift changes were found for amino acids located around the exposed heme edge of cytochrome *c*. The mapping of the affected amide groups appeared to be in good agreement with the contact surface that was indicated in the crystal structure of the same system, and it showed the involvement of hydrophobic rather than electrostatic interactions (*9*).

Even though the molecular structure of the *P. denitrificans* cytochrome c_{552}−cytochrome *c* oxidase complex has not been determined experimentally to date, a computer simulation of the protein−protein interactions was performed in a recent docking study (*10*). On the basis of rigid-body algorithms that include protein surface correlations, electrostatic fitting, and filtering with experimental data as well as functional group distance restraints, mainly charged residues were associated with the surface interactions between cytochrome c_{552} and oxidase. Remarkably, when using either the two-subunit or the four-subunit structure of the *P. denitrificans* oxidase, both of which have been solved by X-ray crystallography (*11*, *12*), the docking results showed a 95° difference in the orientation of the cytochrome c_{552}.

To obtain experimental data regarding the *P. denitrificans* cytochrome c_{552}−cytochrome *c* oxidase interaction surface, we used a 10.5-kDa water-soluble fragment of *P. denitrificans* cytochrome c_{552} (from here on referred to as *cyt* c_{552}) that lacks the helical 30-residue membrane anchor as well as the acidic 40-residue linker segment (*2*). This fragment had been expressed heterologously in *Escherichia coli* (*13*) and was shown to be fully functional in transferring electrons to the native oxidase (*14*). The ^{1}H, ^{15}N, and ^{13}C chemical shifts have been reported for reduced and oxidized *cyt* c_{552} (*15*, *16*), and it was shown that, despite significant spectral differences, the NMR structures were nearly identical in the two redox states (*17*, *18*). To mimic the association with a biologically relevant electron-transfer partner of *cyt* c_{552}, the current study employed the fully functional water-soluble fragment of the cytochrome *c* oxidase subunit II from *P. denitrificans* that contained the copper A center (from here on referred to as Cu_A). The presence of Cu_A caused small chemical shift changes in the TROSY spectra of [^{15}N]-labeled *cyt* c_{552}, which were quantified and analyzed as variations in the electronic environment. The redox-state-independent chemical shift changes were attributed to direct contacts between *cyt* c_{552} and Cu_A. However, differences in chemical shift behavior between the reduced and oxidized systems, as observed in the segment G54-G55-D56, are most likely indirect effects, which we discuss in terms of possible redox-state-dependent conformational changes and alterations in electronic shielding upon protein docking.

MATERIALS AND METHODS

Sample Preparations. [^{15}N]-Labeled *cyt* c_{552} was purified as previously described (*16*). Unlabeled Cu_A was overexpressed in *E. coli* strain JM109 (O. Maneg, unpublished results). Briefly, the region encoding the subunit II residues 103−252 (numbering according to ref *19*) was amplified by PCR, simultaneously introducing a downstream *Hin*dIII and an upstream *Bam*HI restriction site for insertion into the expression vector pQE-30 (Qiagen, Hilden, Germany). A TEV protease recognition site was included in the *Bam*HI site, leading to a cleavable His_6 tag upon protein production. This clone gave expression rates about 20-fold higher than the one described by Lappalainen and co-workers (*20*). As the His_6 tag was not necessary for purification purposes, it was removed during overexpression by co-transforming the bacteria with the plasmid pRK603, which initiates simultaneous production of the TEV protease (*21*). To optimize the cleavage by TEV protease, the bacteria were grown on minimal medium (40 g/L glycerol, 7.5 g/L K_2HPO_4, 5.3 g/L $NaH_2PO_4{\cdot}H_2O$, 2 g/L NH_4Cl, 1 g/L glucose, 1 mM $MgSO_4$, 0.1 mM $CaCl_2$, 10 mL/L trace element solution 1 (*22*), 0.2 μM thiamine, 100 μg/mL ampicillin, 25 μg/mL kanamycin) until mid-log phase and induced for 4 h by addition of IPTG to a final concentration of 0.2 mM. Protein refolding and purification were established according to Lappalainen et al. (*23*). Gel filtration was performed on a Sephacryl HR S200 column (Amersham Bioscience, Freiburg, Germany) in 20 mM Tris at pH 8.0. A final Ni−NTA affinity chromatography step (Qiagen) in 20 mM Bis-Tris buffer at pH 7.0 removed any undesired His_6-tagged Cu_A.

Four NMR samples were prepared, each containing 0.5 mM *cyt* c_{552}, 20 mM potassium phosphate buffer (pH 6.0), 5% (v/v) D_2O, and 0.15 mM 3-(trimethylsilyl)-1-propanesulfonic acid (DSS) as an internal chemical shift reference. Two of the samples additionally contained 2.2 mM Cu_A. One sample with and one sample without Cu_A were reduced by addition of 4 mM sodium ascorbate and repetitive cycles of degassing followed by gassing with argon. The two other samples were oxidized by addition of 5 mM potassium hexacyanoferrate(III).

NMR Experiments and Analysis. All NMR measurements were carried out on a Bruker DRX500 spectrometer equipped with a 5-mm triple-resonance gradient probe, operating at 27 or 7 °C for the reduced and at 27 or 12 °C for the oxidized

samples. 2D sensitivity-enhanced [^{15}N,^{1}H]-TROSY experiments (*24*, *25*) were recorded with 768 and 384 complex data points in the ^{1}H and ^{15}N dimensions, respectively. The spectral widths were set to 7716 (^{1}H) and 5050 Hz (^{15}N). After squared-cosine multiplication and linear prediction up to twice the original size, FIDs were zero-filled and subjected to Fourier transformation to give final datasets of 2K × 2K data points. Protons were referenced to internal DSS, and the ^{15}N dimension was calibrated indirectly with respect to the proton chemical shift (*26*).

After identification of the amide signals on the basis of previous resonance assignments (*15*, *16*) and peak fitting using FELIX (Accelrys Inc., San Diego, U.S.A.), Cu_A-induced changes in the backbone amide proton ($\Delta\delta_{^1HN}$) and nitrogen ($\Delta\delta_{^{15}N}$) chemical shifts of *cyt* c_{552} were determined and combined according to Mulder et al. (*27*), using the expression

$$[(\Delta\delta_{^1HN})^2 + (\Delta\delta_{^{15}N}/6.5)^2]^{1/2} \quad (1)$$

These combined chemical shift changes were normalized to a maximum of 100%. Individual values from measurements performed at two different temperatures were averaged, and residues were color-coded accordingly in the *cyt* c_{552} structure of PDB entry 1QL3 (*28*) using MOLMOL (*29*).

RESULTS AND DISCUSSION

The cytochrome c_{552} of *P. denitrificans* shuttles electrons from the cytochrome bc_1 complex toward cytochrome *c* oxidase. Kinetic studies (data not shown) have pointed out that (i) electrons can be transferred from the water-soluble *cyt* c_{552} fragment (electron donor) to the soluble Cu_A domain (the first electron acceptor of the oxidase) and (ii) the electron transfer between these two isolated fragments is very fast, as was previously also reported for *cyt* c_{552} and the full-size oxidase with turnover numbers reaching 1000 s^{-1} (*14*). However, since the protein contacts are only transient, we have not yet been able to demonstrate a 1:1 complex by gel filtration or microcalorimetry experiments.

To obtain structural data regarding the surface contacts between cytochrome c_{552} and the oxidase, we performed a series of [^{15}N,^{1}H]-TROSY experiments with [^{15}N]-labeled *cyt* c_{552} in the absence and in the presence of unlabeled Cu_A. With this approach, every amide group in *cyt* c_{552} that displays a chemical shift change upon addition of Cu_A yields information about the protein interactions in the short-lived complex formed between the two redox partners. Since electron-transfer rates in biological systems are generally high (*30*), the protein−protein interactions should yield merely subtle changes of the amide resonances when compared to those of free *cyt* c_{552}. Therefore, an excess of Cu_A was used in an attempt to push the association equilibrium toward the bound state of the complex.

Chemical Shift Changes in cyt c_{552} *upon Interaction with* Cu_A. At first, TROSY experiments were performed with either fully reduced or fully oxidized samples at 27 °C. Because of the paramagnetic state of the heme iron in the oxidized protein, the spectra of *cyt* c_{552} at the two redox states are quite different. As expected, the recorded TROSY spectra at 27 °C are essentially identical to the HSQC spectra measured at 25 °C for both the reduced and the oxidized states of free *cyt* c_{552} (*15*, *16*). This confirmed the redox states of the respective systems and allowed the straightforward identification of the amide signals in the TROSY spectra. In addition, TROSY experiments were performed for each redox state at lower temperature, to amplify observed chemical shift changes by forcing the complex into a more long-lived form, and possibly to resolve spectral overlap found at 27 °C. Spectra obtained for free *cyt* c_{552} and for *cyt* c_{552} in the presence of Cu_A are displayed in Figure 1.

Chemical shift changes were observed for backbone as well as side-chain amides of *cyt* c_{552}. The latter, however, were not included in the data analysis, because of the relatively small magnitude of the chemical shift changes, a reduced reproducibility of the results, and complications in the quantification method due to extra splittings that cause additional peaks in the TROSY spectra. In both redox states, the unlabeled Cu_A component produced only small changes in the chemical shift values and line widths of the *cyt* c_{552} amide peaks (Figure 1). This indicates that *cyt* c_{552} basically remained structurally unaltered and predominantly in an uncomplexed state, despite the 4-fold excess of Cu_A. Hence, the interactions between *cyt* c_{552} and Cu_A appear to be rather short-lived protein−protein contacts, which is in agreement with the results of the kinetic assays (*14*; O. Maneg, unpublished results).

For each *cyt* c_{552} amide group, the chemical shift changes in the ^{1}H and ^{15}N dimensions were combined according to eq 1 (*27*). The results thus obtained for each redox state at two different temperatures are displayed in Figure 2. Generally, the occurrence of peak shifts is independent of the temperature, implying that these are not random shifts but signify chemical shielding effects due to the presence of Cu_A. Moreover, mainly visible for the reduced system, the overall magnitude of the peak shifts increased with lower temperature, suggesting that the association equilibrium was shifted to a certain degree toward the bound state by cooling the system.

Upon comparing the relative magnitudes of the Cu_A-induced chemical shift differences for the reduced and oxidized states, much bigger effects were found in the oxidized system (a maximum weighted shift of 0.029 ppm in the reduced system vs 0.138 ppm in the oxidized system, both at 27 °C). However, since the largest effects in the oxidized state appear to be temperature independent, this may not necessarily indicate tighter binding. Alternatively, protein−protein contacts in the oxidized system could influence paramagnetic as well as diamagnetic components contributing to the chemical shift values observed in *cyt* c_{552}, whereas in the reduced form the chemical shift changes are determined solely by diamagnetic components (*7*). For each redox state, the chemical shift changes were normalized with respect to the maximal shift and, wherever possible, the values were averaged over both temperatures. To graphically visualize the *cyt* c_{552} residues that were influenced by the presence of Cu_A, these averages were used in Figure 3 to color-code the *cyt* c_{552} structure (*28*). As anticipated, the residues that are most strongly influenced are all located on the *cyt* c_{552} surface.

Contact Area on the cyt c_{552} *Surface*. Strong similarities were found between the reduced and oxidized systems (Figure 3), implying that the contact site between the two redox partners is not dependent on the redox state. In both

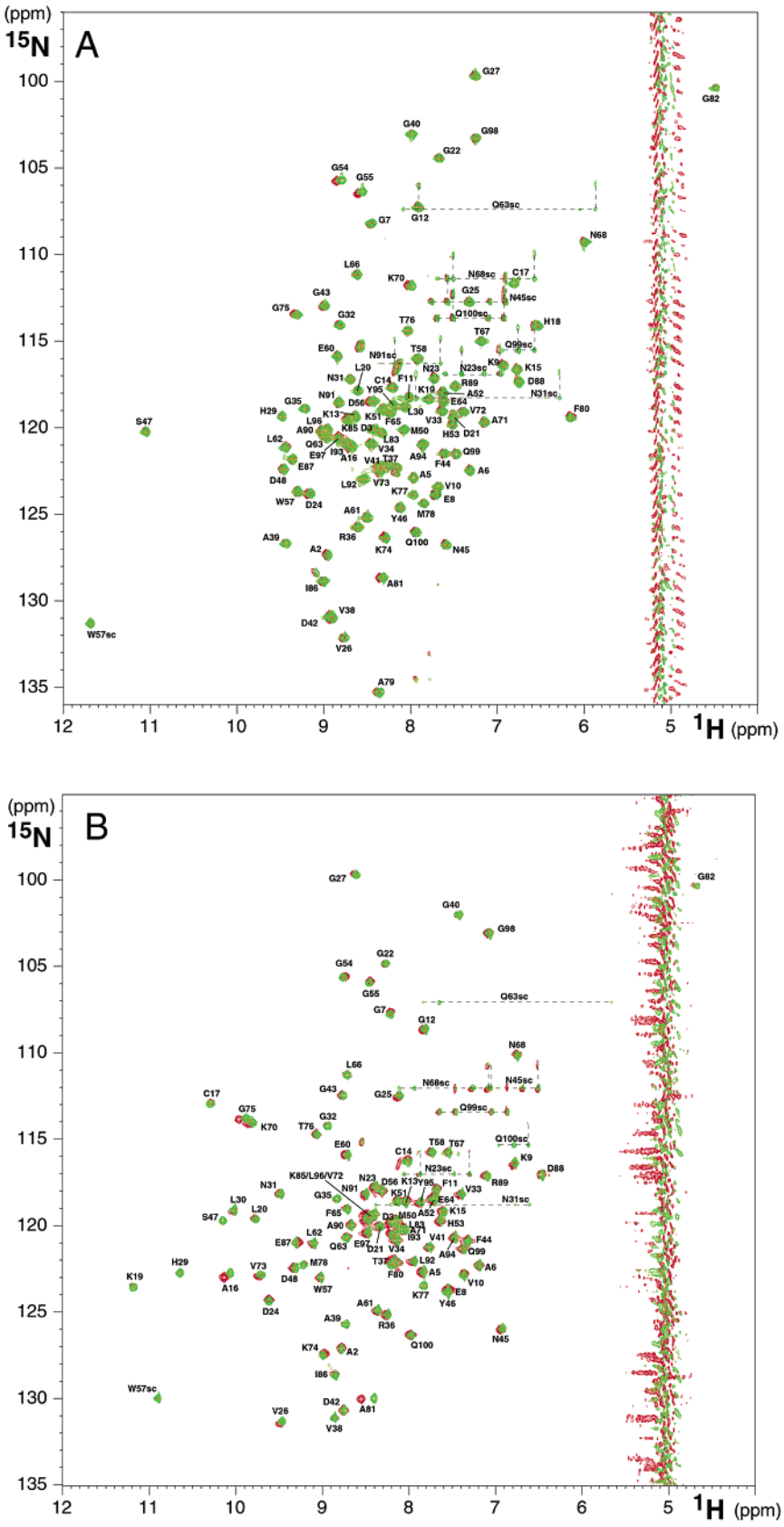

FIGURE 1: 2D [^{15}N,^{1}H]-TROSY spectra were recorded with [^{15}N]-labeled *cyt* c_{552} in the absence (green) and in the presence (red) of unlabeled Cu_A. Spectra of (A) fully reduced samples at 7 °C and (B) fully oxidized samples at 12 °C are shown. The backbone and side-chain assignments are indicated (*15*, *16*).

oxidation states, residues A16, K70, G75, and A81 display pronounced amide shifts in the presence of Cu_A. A more detailed analysis of the results from the individual experiments (see Figure 2) reveals that residues D24, V26, A79, and F80, and possibly also G25, G27, and G82, are involved in direct contacts with Cu_A as well. This gives rise to a more

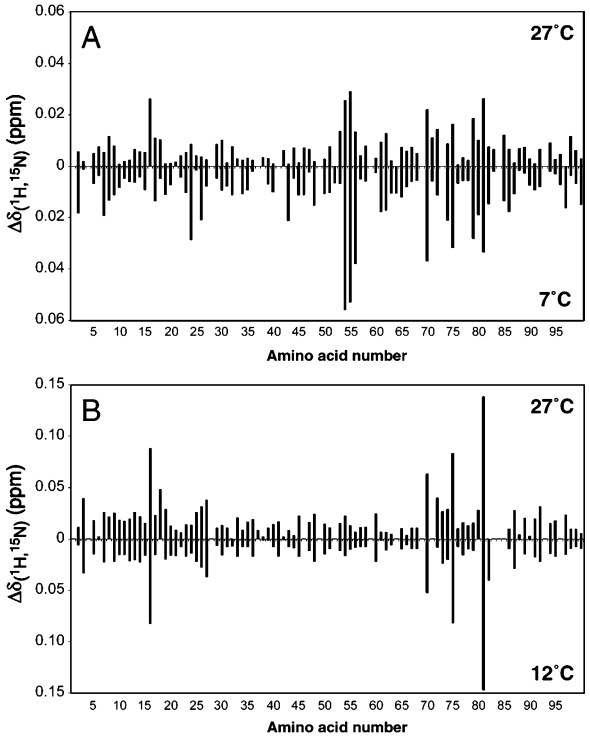

FIGURE 2: Overview of the combined backbone amide ^1H and ^{15}N chemical shift changes which were observed for [^{15}N]-labeled *cyt* c_{552} upon addition of excess Cu_A. Panel A represents the reduced system at 27 (top) and 7 °C (bottom), and panel B represents the oxidized system at 27 (top) and 12 °C (bottom).

or less contiguous interaction surface that is centered around the heme cleft (which is likely to mediate the electron transfer) and surrounded by several positively charged lysine residues (Figure 4).

By using approaches and complexes similar to those presented here, NMR chemical shift mapping has also been performed on the horse cytochrome *c*−pea plastocyanin complex (*7*) and on yeast cytochrome *c* in the presence of its peroxidase (*8*). Comparable to our results, it was shown that residues surrounding the exposed edge of the cytochrome *c* heme moiety were most strongly affected, indicative of the observation of biologically relevant protein contacts. Furthermore, crystallographic data obtained for the yeast complexes cytochrome *c*−cytochrome bc_1 (*31*) and cytochrome *c*−cytochrome *c* peroxidase (*9*) produced similar results, implying that not only NMR spectroscopy but, in certain cases, also X-ray crystallography (which usually requires conditions that provide a stable complex) may be used to study transient protein−protein interactions.

In contrast to the docking results that suggest a complex formation based on multiple electrostatic contacts between *P. denitrificans* cytochrome c_{552} and cytochrome *c* oxidase (*10*), only one positively charged *cyt* c_{552} residue (K70) displays a backbone amide shift due to the presence of Cu_A, whereas the rest of the affected residues are uncharged. However, our results are in good agreement with a previously proposed model for the complex formation between *P. denitrificans* cytochrome *c* and cytochrome *c* oxidase (*4*). In this model, the positively charged lysine residues that are arranged on the cytochrome c_{552} surface around the heme cleft (Figure 4) provide the basis for long-range electrostatic attractions with patches of opposite charge above the Cu_A center of the oxidase. Formation of this encounter complex is followed by a step of molecular rearrangement that involves mostly uncharged residues on the interaction surfaces of both redox partners, yielding close intermolecular contacts around the heme group for optimal electron transfer (*4*). Thus, most of the *cyt* c_{552} lysine residues which the docking study indicated to be involved in the protein association (*10*) apparently contribute to the encounter complex, but are not necessarily part of the final protein−protein contact surface.

Hence, we propose the following interaction scenario between *cyt* c_{552} and Cu_A. On the *cyt* c_{552} surface, the positively charged lysines surrounding the heme cleft can be roughly divided into an inner ring (K13, K15, K70, and K77) and an outer ring (K9, K19, K51, K74, and K85). The outer ring of lysines lines the periphery of this surface area (see Figure 4), with intramolecular salt bridges present between K19 and D21 (4.4 Å), K51 and D48 (3.6 Å), and K85 and D88 (4.6 Å). While these lysines add to the polarization of the general surface potential that represents the basis for the encounter complex formed with Cu_A, the inner ring lysines probably contribute the most to these electrostatic interactions that involve 2−3 charges on each protein surface (O. Maneg, unpublished results). In a second step, van der Waals interactions between the two redox partners, involving residues A16, D24, G25, V26, G27, K70, G75, A79, F80, A81, and G82 on the *cyt* c_{552} surface, cause an intermolecular rearrangement. At this point, the redox partners are positioned in such a way that an electron can be transferred from the heme moiety of *cyt* c_{552} through the W121 indole ring on the Cu_A surface to the binuclear copper A center.

The influence of charged residues on the complex formation and electron-transfer efficiency has been established previously also for various other electron-transfer proteins. For instance, the importance of the general surface potential was demonstrated for long-range interactions between the reaction center of *Rhodobacter sphaeroides* and soluble *c*-type cytochromes (*32*). Moreover, single mutation studies on the nine lysine residues in the *cyt* c_{552} fragment from *P. denitrificans* (*14*) generally led, in an assay with oxidase, to a 3−5-fold loss of affinity (K_M values increased from 3.2 to 14.8 μM for K70I) and a concomitant decrease of k_{cat}. However, no outstanding role of K70 could be shown under steady-state conditions that monitor the complete electron-transfer process, including long-range attraction, fine-tuning, electron transfer, and dissociation.

To date, no mutational studies have focused on the hydrophobic residues that are clustered around the *cyt* c_{552} heme crevice, but the data presented here strongly support the existence of a second reaction step with a protein reorientation involving hydrophobic interactions as part of the electron-transfer process. Previously, Witt et al. (*4*) demonstrated that hydrophobic residues surrounding the electron entry-site (W121) of the *P. denitrificans* oxidase did not affect the binding of horse heart cytochrome *c* but did influence k_{cat} under turnover conditions. Furthermore, on the surface of the plastocyanin from *Phormidium laminosum*, a hydrophobic patch was identified to be responsible for the interaction with its physiological redox partner cytochrome *f* (*33*). In other studies, binding of either *Anabaena* sp. PCC 7119 cytochrome c_6 (*34*) or *Prochloro-*

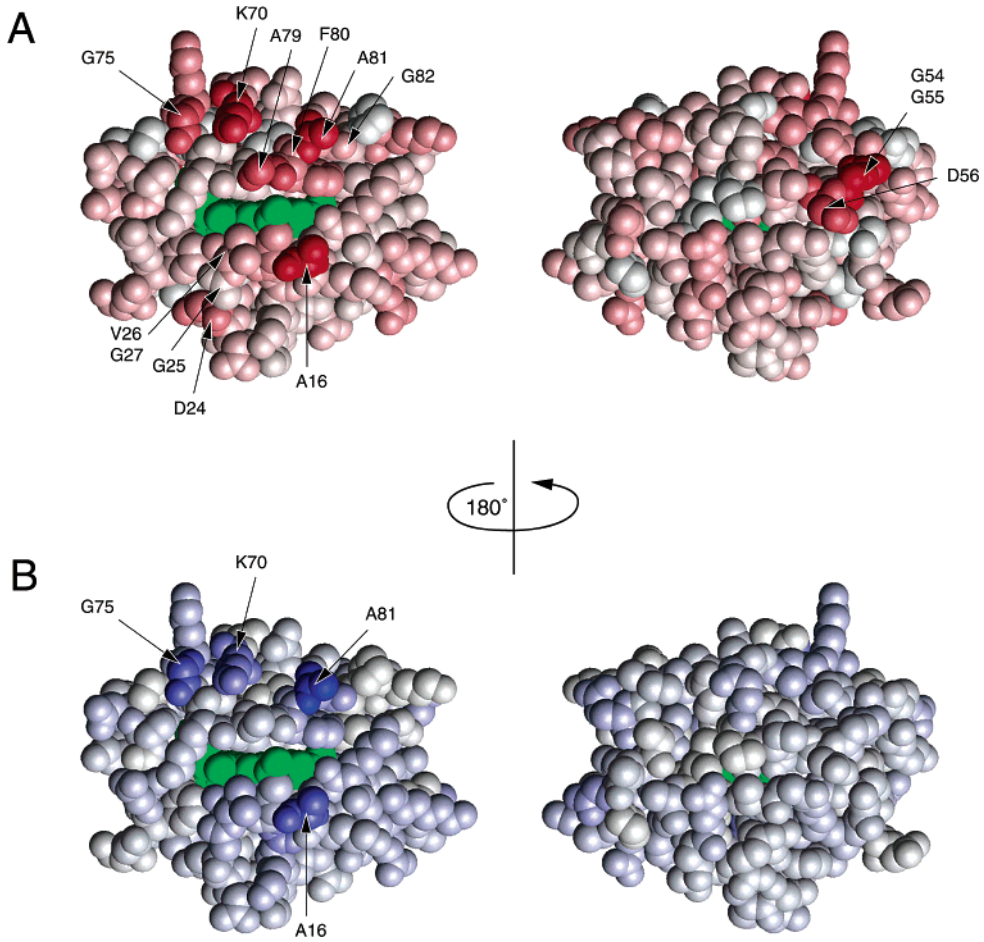

FIGURE 3: The *cyt* c_{552} structure (PDB entry 1QL3; *28*) is color-coded according to the averages of the weighted backbone amide chemical shift changes as depicted in Figure 2. Panels A and B show the residues affected in the reduced (red) and the oxidized (blue) systems, respectively. For clarity, not only the affected backbone amides are highlighted, but the respective amino acids have been colored entirely. The heme moiety is shown in green; the molecule on the right is rotated by 180° about the vertical axis.

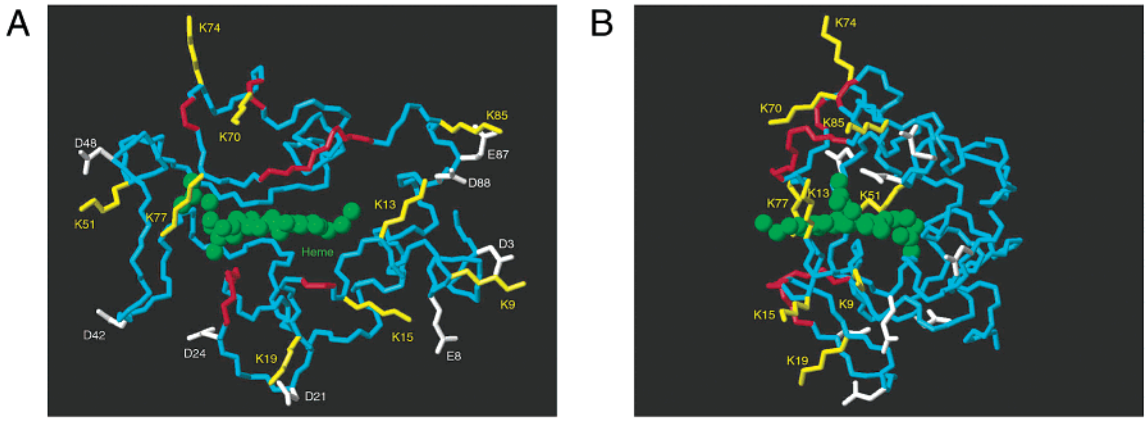

FIGURE 4: Graphic representation of the *cyt* c_{552} backbone fold (PDB entry 1QL3; *28*) from the front (A) and rotated by 90° about the vertical axis (B). Highlighted are all lysine side chains (yellow) as well as negatively charged surface residues (white) that are visible from the front. Residues that display chemical shift changes due to direct contacts with Cu_A (i.e., A16, D24, G25, V26, G27, K70, G75, A79, F80, A81, and G82) are indicated by a red backbone color.

thrix hollandica plastocyanin (*35*) to cytochrome *f* from *P. laminosum* revealed a clear ionic strength dependency, showing that the complex formation is mediated by charged surface residues, even though mainly hydrophobic residues were identified as direct interaction sites.

It is interesting to note that, although no electron transfer is possible under the experimental conditions applied here, transient complex formation apparently still took place. Consequently, the proposed electrostatic interaction and intermolecular rearrangement steps leading to hydrophobic protein contacts do not depend on the oxidation states of the individual components. This implies that, in the native system, transient contacts between the membrane-bound electron donor and acceptor occur which are not necessarily

productive but do allow electron transfer whenever a suitable driving force is present. Hence, the hydrophobic contacts between the electron-transfer partners could be a prerequisite for the electron-transfer reaction to take place.

Indirect Effects in cyt c_{552} upon Association with Cu_A. Although the results obtained for both redox states are very similar, there is one remarkable difference: as can be seen in Figures 2 and 3, the influence of Cu_A on the backbone amide resonances of the segment G54-G55-D56 is pronounced in the reduced state yet completely absent in the oxidized state of *cyt* c_{552}. G54-G55-D56 is part of the loop G54-T58 connecting the helices II (residues 48−53) and III (residues 59−67). This loop extends nearly parallel to the plane of the porphyrin ring, but on the opposite face of *cyt* c_{552} relative to the exposed heme edge. Since it is highly unlikely that the binding of Cu_A involves direct contacts with residues on opposite sides of *cyt* c_{552}, the chemical shift changes found in this region of the protein probably reflect indirect effects due to the interaction between the two proteins. Although our data do not provide an immediate explanation, structural and electronic arguments may be considered.

Many eukaryotic cytochromes *c* exhibit common redox-state-specific conformational distinctions (*36*). These may be related to redox-state-dependent differences upon association with their respective oxidases. Similarly, a conformational rearrangement or differential dynamics in the region G54-G55-D56 could be the cause for the chemical shift changes observed in the presence of Cu_A. Although differences in backbone accessibility have been reported for reduced and oxidized *cyt* c_{552} from *P. denitrificans*, the backbone structure as well as dynamics (as studied by relaxation measurements) showed no major variations (*18*). Nevertheless, careful comparison of the NMR structure ensembles of reduced and oxidized *cyt* c_{552} (PDB entries 1I6D and 1I6E) indicates a minor displacement of the backbone segment G54-G55-D56 upon oxidation, as well as distinct orientations of the adjacent H53 imidazole ring. In principle, these small differences between the reduced and oxidized states could be amplified upon interaction with Cu_A, thus leading to the observed effects. The crystallography data of reduced and oxidized *cyt* c_{552} (PDB entries 1QL3 and 1QL4; *28*) support a model where small redox-state-dependent structural distinctions may be enhanced upon binding to an electron-transfer partner, as they indicated a higher conformational disorder from G40 to D56 in the oxidized protein form. However, the crystallography and NMR data also show some discrepancies, as (i) the conformation of the G54-G55-D56 segment is not redox-state-dependent in the X-ray structures and (ii) the NMR experiments did not reveal an oxidation-state-dependent backbone flexibility.

Alternatively, the observed redox-state-specific effects could be explained by small changes in the heme moiety due to oxidation of the system. For instance, the propionate group of the heme pyrrole ring A in yeast iso-1-cytochrome *c* moves slightly upon oxidation, causing a reorganization of hydrogen bonds and bound water molecules in its immediate vicinity (*37*). Similarly, the heme group of *cyt* c_{552} might be structurally altered or slightly shifted as a whole inside the protein pocket upon interaction with Cu_A. However, there are arguments that seem to preclude such conformational rearrangements: (i) the structure and position of the heme group of *cyt* c_{552} from *P. denitrificans* remains unaltered in both redox states (*18*, *28*) and (ii) no additional chemical shift changes have been observed for other amide protons in the vicinity of the heme group, such as V38 or S47.

Since no significant conformational changes were detected in the NMR spectra of *cyt* c_{552} upon Cu_A binding (Figure 1), the occurrence of the observed effects on the opposite side of the protein could also relate to the difference in the number of electrons in the redox system. Compared to the oxidized system, the fully reduced system accommodates one additional electron in each redox partner. Hence, an extra negative charge is dispersed over the entire heme moiety of *cyt* c_{552}, possibly including the propionate groups (*38*). Assuming that the *cyt* c_{552}−Cu_A surface contacts initiate a reorganization of the electron density within the protein interior whenever electron transfer is in principle allowed, this could result in a shift of the electron density in the reduced state toward the back of the heme cleft, possibly exerting an indirect influence on the amide groups of residues G54, G55, and D56. The fact that the fluorescence spectra of reduced and oxidized *cyt* c_{552}, despite the two forms having identical conformations, previously revealed a significant difference in the electronic environment of the adjacent W57 indole ring (*18*) supports a possible influence of the electronic state of the heme moiety on this part of the *cyt* c_{552} molecule.

CONCLUSIONS

In this study, small yet reproducible chemical shift changes have been observed for *cyt* c_{552} upon interaction with the soluble Cu_A domain. Comparable effects were found for both the completely reduced and oxidized systems, indicating that the protein interaction does not depend on the redox states of the electron-transfer partners. This suggests a dynamic mode of action, whereby the two proteins encounter each other frequently and allow electron transfer whenever a suitable driving force is present. Furthermore, the NMR results indicate the presence of a hydrophobic contact patch on the *cyt* c_{552} surface, surrounded by several positively charged lysine side chains, which agrees with the two-step model for complex formation proposed by Witt et al. (*4*). According to this model, the two proteins initially attract and orient each other via electrostatic forces, as was confirmed previously (*14*). Once the redox partners are in close proximity, van der Waals contacts between hydrophobic side chains cause an orientational fine-tuning that allows electron transfer to take place.

Aside from one example from the realm of cyanobacteria (*33*), this work contains the only description of a transient complex between two physiological respiratory electron-transfer partners studied by NMR. In the native system, both proteins are membrane-embedded and organized in a supercomplex; these additional structural determinants allow for very high reaction rates despite very weak interactions.

ACKNOWLEDGMENT

D. Waugh is acknowledged for making the pRK603 plasmid available to us. The authors thank B. Reincke for providing the purified [^{15}N]-labeled *cyt* c_{552}, P. Schmitt for technical assistance, and G. Yalloway for help with the

reduction of the NMR samples. All NMR experiments were performed at the Center for Biomolecular Magnetic Resonance at the University of Frankfurt.

REFERENCES

1. Berry, E. A., and Trumpower, B. L. (1985) *J. Biol. Chem. 260*, 2458−2467.
2. Turba, A., Jetzek, M., and Ludwig, B. (1995) *Eur. J. Biochem. 231*, 259−265.
3. Witt, H., Malatesta, F., Nicoletti, F., Brunori, M., and Ludwig, B. (1998) *Eur. J. Biochem. 251*, 367−373.
4. Witt, H., Malatesta, F., Nicoletti, F., Brunori, M., and Ludwig, B. (1998) *J. Biol. Chem. 273*, 5132−5136.
5. Hall, D. A., Vander Kooi, C. W., Stasik, C. N., Stevens, S. Y., Zuiderweg, E. R. P., and Matthews, R. G. (2001) *Proc. Natl. Acad. Sci. U.S.A. 98*, 9521−9526.
6. Zuiderweg, E. R. P. (2002) *Biochemistry 41*, 1−7.
7. Ubbink, M., and Bendall, D. S. (1997) *Biochemistry 36*, 6326−6335.
8. Worrall, J. A. R., Kolczak, U., Canters, G. W., and Ubbink, M. (2001) *Biochemistry 40*, 7069−7076.
9. Pelletier, H., and Kraut, J. (1992) *Science 258*, 1748−1755.
10. Flöck, D., and Helms, V. (2002) *Proteins 47*, 75−85.
11. Ostermeier, C., Harrenga, A., Ermler, U., and Michel, H. (1997) *Proc. Natl. Acad. Sci. U.S.A. 94*, 10547−10553.
12. Harrenga, A., and Michel, H. (1999) *J. Biol. Chem. 274*, 33296−33299.
13. Reincke, B., Thöny-Meyer, L., Dannehl, C., Odenwald, A., Aidim, M., Witt, H., Rüterjans, H., and Ludwig, B. (1999) *Biochim. Biophys. Acta 1411*, 114−120.
14. Drosou, V., Reincke, B., Schneider, M., and Ludwig, B. (2002) *Biochemistry 41*, 10629−10634.
15. Lücke, C., Reincke, B., Löhr, F., Pristovšek, P., Ludwig, B., and Rüterjans, H. (2000) *J. Biomol. NMR 18*, 365−366.
16. Pristovšek, P., Lücke, C., Reincke, B., Löhr, F., Ludwig, B., and Rüterjans, H. (2000) *J. Biomol. NMR 16*, 353−354.
17. Pristovšek, P., Lücke, C., Reincke, B., Ludwig, B., and Rüterjans, H. (2000) *Eur. J. Biochem. 267*, 4205−4212.
18. Reincke, B., Pérez, C., Pristovšek, P., Lücke, C., Ludwig, C., Löhr, F., Rogov, V. V., Ludwig, B., and Rüterjans, H., (2001) *Biochemistry 40*, 12312−12320.
19. Iwata, S., Ostermeier, C., Ludwig, B., and Michel, H. (1995) *Nature 376*, 660−669.
20. Lappalainen, P., Watmough, N. J., Greenwood, C., and Saraste, M. (1995) *Biochemistry 34*, 5824−5830.
21. Kapust, R. B., and Waugh, D. S. (2000) *Protein Expr. Purif. 19*, 312−318.
22. Coligan, J. E., Dunn, B. M., Ploegh, H. L., Speicher, D. W., and Wingfield, P. T. (1995) in *Current Protocols in Protein Science* (Benson Chanda, V., Series Ed.), John Wiley and Sons Inc., New York.
23. Lappalainen, P., Aasa, R., Malmström, B. G., and Saraste, M. (1993) *J. Biol. Chem. 268*, 26416−26421.
24. Pervushin, K. V., Wider, G., and Wüthrich, K. (1998) *J. Biomol. NMR 12*, 345−348.
25. Czisch, M., and Boelens, R. (1998) *J. Magn. Reson. 134*, 158−160.
26. Wishart, D. S., Bigam, C. G., Yao, J., Abildgaard, F., Dyson, H. J., Oldfield, E., Markley, J. L., and Sykes, B. (1995) *J. Biomol. NMR 6*, 135−140.
27. Mulder, F. A. A., Schipper, D., Bott, R., and Boelens, R. (1999) *J. Mol. Biol. 292*, 111−123.
28. Harrenga, A., Reincke, B., Rüterjans, H., Ludwig, B., and Michel, H. (2000) *J. Mol. Biol. 295*, 667−678.
29. Koradi, R., and Billeter, M. (1998) *P.D.B. Newsl. 84*, 5−7.
30. Gray, H. B., and Winkler, J. R. (1996) *Annu. Rev. Biochem. 65*, 537−561.
31. Lange, C., and Hunte, C. (2002) *Proc. Natl. Acad. Sci. U.S.A. 99*, 2800−2805.
32. Tiede, D. M., Vashishta, A. C., and Gunner, M. R. (1993) *Biochemistry 32*, 4515−4531.
33. Crowley, P. B., Otting, G., Schlarb-Ridley, B. G., Canters, G. W., and Ubbink, M. (2001) *J. Am. Chem. Soc. 123*, 10444−10453.
34. Crowley, P. B., Diaz-Quintana, A., Molina-Heredia, F. P., Nieto, P., Sutter, M., Haehnel, W., De la Rossa, M. A., and Ubbink, M. (2002) *J. Biol. Chem. 277*, 48685−48689.
35. Crowley, P. B., Vintonenko, N., Bullerjahn, G. S., and Ubbink, M. (2002) *Biochemistry 41*, 15698−15705.
36. Calvert, J. F., Hill, J. L., and Dong, A. (1997) *Arch. Biochem. Biophys. 346*, 287−293
37. Berghuis, A. M., and Brayer, G. D. (1992) *J. Mol. Biol. 223*, 959−976.
38. Johansson, M. K., Blomberg, M. A. R., Sundholm, D., and Wikström, M. (2002) *Biochim. Biophys. Acta 1553*, 183−187.

BI027198F